Separation Science and Technology
Publication details, including instructions for authors and subscription information:
http://www.informaworld.com/smpp/title~content=t713708471

MICROFLOTATION OF FINE OIL DROPLETS BY SMALL AIR BUBBLES: EXPERIMENT AND THEORY

José A. Ramirez[a]; Robert H. Davis[b]
[a] Virox Technologies, Mississauga, Canada [b] Department of Chemical Engineering, University of Colorado, Boulder, Colorado, U.S.A.

Online publication date: 13 February 2001

To cite this Article Ramirez, José A. and Davis, Robert H.(2001) 'MICROFLOTATION OF FINE OIL DROPLETS BY SMALL AIR BUBBLES: EXPERIMENT AND THEORY', Separation Science and Technology, 36: 1, 1 — 15
To link to this Article: DOI: 10.1081/SS-100000847
URL: http://dx.doi.org/10.1081/SS-100000847

SEPARATION SCIENCE AND TECHNOLOGY, 36(1), 1–15 (2001)

MICROFLOTATION OF FINE OIL DROPLETS BY SMALL AIR BUBBLES: EXPERIMENT AND THEORY

José A. Ramirez* **and Robert H. Davis†**

Department of Chemical Engineering, University of Colorado, Boulder, Colorado 80309-0424

ABSTRACT

A trajectory analysis accounting for hydrodynamic interactions and van der Waals attractions was performed to predict the kinetic constant for capture of fine but non-Brownian oil droplets by small air bubbles under creeping-flow conditions. For the range of bubble ($40\ \mu\text{m} \leq 2a_1 \leq 80\ \mu\text{m}$) and droplet ($3\ \mu\text{m} \leq 2a_2 \leq 20\ \mu\text{m}$) diameters of interest, the theoretical kinetic constant scales as $k \propto \phi a_1^{-0.86} a_2^{1.21}$, where ϕ is the gas holdup, a_1 is the bubble radius, and a_2 is the droplet radius. Experiments with a batch flotation cell support these scalings, but the quantitative predictions for the capture rate are about three times higher than the measured values. Smaller bubbles are more efficient collectors because they have higher surface area per volume and cause weaker hydrodynamic interactions, whereas smaller droplets are floated less efficiently because they tend to flow around the rising bubbles.

*Present address: Virox Technologies, 6705 Millcreek Drive, Unit 4, Mississauga, ON L5N 5M4, Canada.

†Address correspondence to Robert H. Davis. E-mail: robert.davis@colorado.edu

Key Words: Flotation; Microflotation; Droplets; Bubbles.

INTRODUCTION

Microflotation refers to the removal of fine suspended matter from water using small gas bubbles with diameters of approximately 100 μm or less. Such small bubbles capture even smaller particles more efficiently than do the millimeter-size bubbles that are typical of conventional flotation processes (1). For proper design of microflotation devices, accurate expressions or data for the particle capture rate are needed.

One of the first experimental studies on microflotation was performed by Rubin et al. (2), who evaluated the removal efficiency of bacteria and algae from aqueous culture media in a batch flotation cell by microscopic nitrogen bubbles. Their emphasis was on finding the chemical collector and solution pH that would maximize the cell removal efficiency. Microflotation experiments for clay suspensions (3,4), colloidal humic acid (5), microcrystalline cellulose (6), and dyes (7) are a few examples of similar studies.

Experimental corroboration of model predictions for the microflotation rate has been attempted with limited success by Reay and Ratcliff (8) and later by Collins and Jameson (9). In both cases, the predicted dependence of the flotation kinetics on the suspended particle size was not observed experimentally. For the microfiltration of nearly neutrally buoyant polystyrene spheres, the experimental dependence of the kinetic constant, k, on the particle radius, a_2, was found in both studies to be of the form $k \propto a_2^{1.5}$; in contrast, the model-predicted dependence is $k \propto a_2^{2.0}$ (8).

The flotation of oil-in-water dispersions has also received considerable attention. Angelidou et al. (10) compared the values obtained for the kinetic constant to the convective and diffusive models for Stokes flow of Reay and Ratcliff (11). Even though they employed rather large non-Stokesian bubbles of mean diameter of about 150 μm, they measured kinetic constants which are within the predicted ranges. Rulev et al. (12) employed even larger bubbles, with diameters ranging from 350 to 460 μm, and fitted an expression for the collection efficiency in powers of the droplet–bubble size ratio. Okada et al. (13) separately measured the zeta potentials of bubbles and oil droplets and examined their effects on the collection efficiency through measurements in batch flotation experiments. They employed bubbles of approximately 500 μm in diameter in media of relatively low ionic strength (10^{-5} to 10^{-2} M). Medrzycka (14) used bubbles of diameters between 200 and 400 μm in his oil flotation experiments, observing good agreement between the measured flotation rates and those predicted from an interception model.

In the present work, microscopic gas dispersions (with bubbles of diameter smaller than 100 μm) were employed in a batch flotation cell to remove suspended

oil droplets from water. The measured collection efficiencies are compared to those predicted from the model of Loewenberg and Davis (1). Unlike previous studies, high ionic strength was used to assure that the electrostatic interactions between the bubbles and suspended droplets were minimized. In this way, we focused our study on the bubble–droplet hydrodynamic interactions and their effect on the collection efficiency.

THEORY

We consider a dilute suspension of droplets (with concentration less than approximately 1000 mg/L) being floated with air bubbles at very low gas holdups (no higher than 10%). The rate of removal of suspended droplets from the bulk liquid is given by (1)

$$-\frac{dn_2}{dt} = J_{12} \tag{1}$$

where n_2 is the number of suspended droplets of a given size category per unit volume in the suspension and J_{12} is the droplet collection rate per unit volume. The latter is written as the product of the collision rate in the absence of bubble–droplet interactions, J_{12}^o, and the bubble–droplet capture efficiency, E_{12}:

$$J_{12} = J_{12}^o E_{12} \tag{2}$$

The Smoluchowski flux, J_{12}^o, is typically written as (1)

$$J_{12}^o = n_1 n_2 \pi (a_1 + a_2)^2 V_{12}^o \tag{3}$$

where n_1 is the number density of bubbles of a given size category in the suspension, a_1 is the bubble radius, and V_{12}^o is the far-field relative velocity between the bubble and droplet.

For a monodisperse bubble distribution a_1, integration of Equation (1) yields

$$n_2 = n_{2o}\, e^{-k_m t} \tag{4}$$

where n_{2o} is the initial number of particles of radius a_2 per unit volume and the first-order kinetic constant is given by

$$k_m = n_1 \pi (a_1 + a_2)^2 V_{12}^o E_{12} \tag{5}$$

However, the polydisperse nature of the bubbles should be taken into account. We assume that the bubble size distribution in the flotation cell is described by a normalized distribution function, $f(r_1)$, such that the number density of bubbles whose radii are in the range $(r_1, r_1 + dr_1)$ is given by

$$dn_1 = n_{1o} f(r_1)\, dr_1 \tag{6}$$

MARCEL DEKKER, INC.
270 Madison Avenue, New York, New York 10016

where n_{1o} is the total bubble number density in the suspension. The function $f(r_1)$ satisfies the normalization condition

$$\int_{a_{1,1}}^{a_{1,N}} f(r_1)\,dr_1 = 1 \tag{7}$$

where $a_{1,1}$ and $a_{1,N}$ are the smallest and largest bubble sizes contained in the gas dispersion, respectively. The rate of removal of droplets of radius a_2 by the polydispersed bubbles is then given by

$$-\frac{dn_2}{dt} = n_{1o}n_2\left[\int_{a_{1,1}}^{a_{1,N}} \pi(r_1 + a_2)^2 V_{12}^o(r_1, a_2)E_{12}(r_1, a_2)f(r_1)\,dr_1\right] \tag{8}$$

Integration of Equation (8) yields the same exponential decay of Equation (4), but with k_m replaced by

$$k = n_{1o}\int_{a_{1,1}}^{a_{1,N}} \pi(r_1 + a_2)^2 V_{12}^o(r_1, a_2)E_{12}(r_1, a_2)f(r_1)\,dr_1 \tag{9}$$

The capture efficiency, E_{12}, accounts for the hydrodynamic and molecular interactions between the bubble and a suspended droplet, which affect their relative motion and attachment. When the bubbles and drops are non-Brownian (i.e., with diameters of a few microns or greater), the capture efficiency is numerically calculated from a trajectory analysis (1,15), in which the capture cross-section is found from determining the limiting trajectory that demarcates capture and separation. When Brownian motion is important, then the convection–dispersion equation must be solved to find the capture rate (16).

In the experiments of this paper, the drops and bubbles are sufficiently large to be non-Brownian but sufficiently small for inertia and deformation to be neglible. Following Loewenberg and Davis (1), the two-sphere mobility functions accounting for hydrodynamic interactions in Stokes flow were used to find the capture efficiency from a trajectory analysis. It was assumed that the bubbles behaved as having completely rigid interfaces. In practice, this constitutes a reasonable approximation for these types of experiments (2), because a very high concentration of frothing agent (isopropanol) was used to achieve sufficiently small bubbles. The frothing agent is a surfactant that lowers the interfacial tension and reduces the interfacial mobility through Marangoni stresses (17,18). Because salt was employed, it was further assumed that any elecrostatic repulsion was repressed and that van der Waals attraction pulled the drop and bubble together when they became close. Capture was assumed to occur on contact, as the oil drops are hydrophobic.

Several calculations over the range of bubble and droplet sizes of interest were performed to determine the predicted collection efficiencies. All transport properties were evaluated at room temperature ($T = 298$ K), and a typical value of $A_{\mathrm{H}} = 4 \times 10^{-21} J$ (1) was used for the Hamaker constant. The results are shown in Figure 1. The collection efficiency decreases with increasing bubble size,

MARCEL DEKKER, INC.
270 Madison Avenue, New York, New York 10016

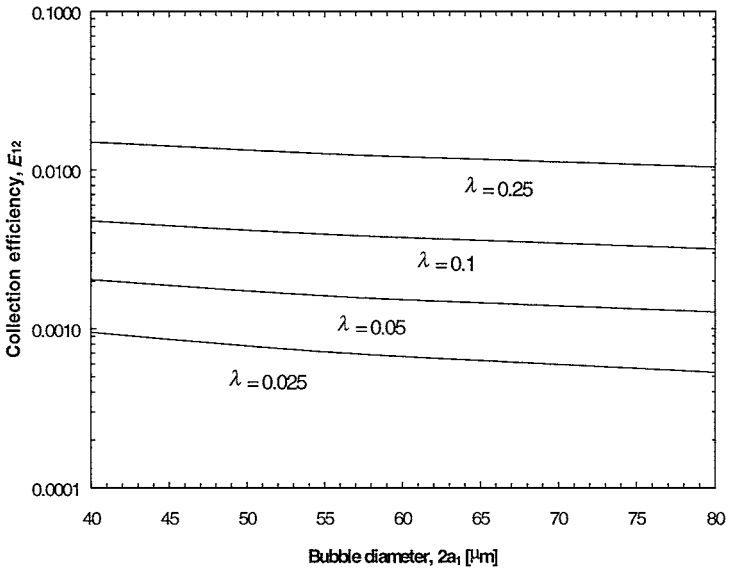

Figure 1. Model-predicted collection efficiencies in the range of bubble sizes of interest, for several size ratios $\lambda = a_2/a_1$. The bubble interfaces were assumed completely rigid, and a value of $4 \times 10^{-21} J$ was used for the Hamaker constant. Transport property values at $T = 298$ K were used.

because the attractive van der Waals forces (which pull the bubble and drop together when sufficiently close) do not increase as strongly with increasing bubble size as do the hydrodynamic forces that resist the relative approach of the drop and bubble. The collection efficiency also decreases with decreasing drop-to-bubble size ratio, $\lambda = a_2/a_1$, as hydrodynamic interactions cause smaller drops to flow around the bubble. The capture efficiency, E_{12}, is well described by the form: $E_{12} = 0.586 a_1^{-1.86} a_2^{1.21}$, with both a_1 and a_2 in microns. In addition, the relative velocity between a well-separated bubble and droplet, V_{12}^o, is given by Stokes law, which for the present conditions reduces to $V_{12}^o = 5.45 \times 10^{-5} a_1^2$, with a_1 in microns and V_{12}^o in cm/s. Note that the contribution from the isolated velocity of the small droplets is negligible relative to the bubble rise velocity, because they are relatively small and nearly neutrally buoyant.

MATERIALS AND METHODS

A synthetic lubricating oil-in-water (commercial brand 3-in-1 Household oil, Boyle-Midway, Inc.) dispersion was prepared by adding the oil to deionized water (resistance 18.3 MΩ · cm) and mixing at medium speed in a blender

MARCEL DEKKER, INC.
270 Madison Avenue, New York, New York 10016

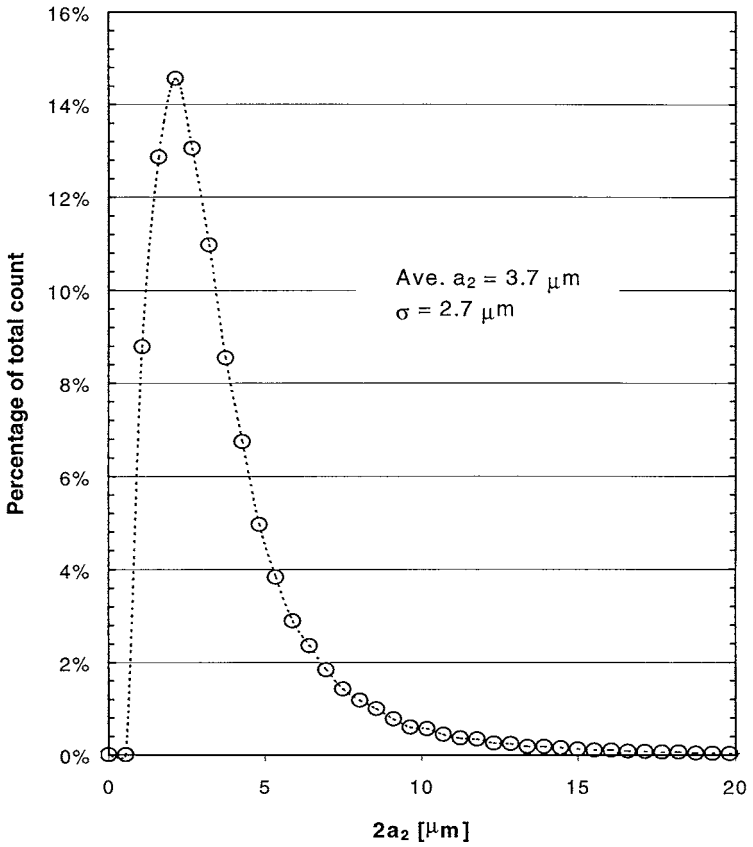

Figure 2. Size distribution of oil-in-water dispersion used in the experiments.

(Osterizer Model 890-28M) for 30 s. The resulting dispersion had a mean droplet diameter of 4 μm on a number basis (see Fig. 2), as measured by a Coulter Multisizer, using a 50-μm orifice tube. Isopropanol (ISA, Aldrich, Cat. No. 10,982-7) was used as a frothing agent and to facilitate the production of small gas bubbles in the cell. Previous work has shown that ethanol as a frothing agent is also effective in reducing the bubble size and thereby increasing the capture efficiency of colloidal particles (19). The cationic surfactant cethyldimethylammonium bromide (CDAB, Cat. No. 21187-1000 Acros Organics) was tested as a "collector" chemical in a few experiments. Collectors are commonly used (particularly in the flotation of hydrophilic matter) to render the particles more hydrophobic and thus increase their probability of attachment (8,9). However, the cationic surfactant decreased the flotation rate of the hydrophobic oil drops used here, possibly

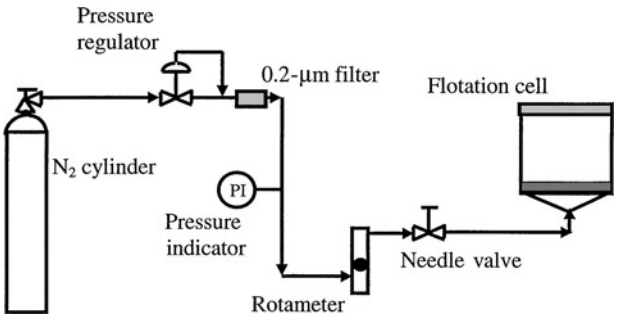

Figure 3. Schematic of experimental apparatus employed in the experiments.

due to steric effects, and so it was not used for the remainder of the reported experiments.

Batch flotation experiments were performed using the experimental setup shown in Figure 3. The gas bubbles were generated by controlling the flow of nitrogen gas through a porous frit located at the bottom of the flotation cell. A constant gas pressure was maintained by using a pressure regulator (Victor, GPT 270D–250), and the flow was manually controlled and monitored with a needle valve (Nupro Series B) and rotameter (Matheson, 601 tube) assembly. Two types of flotation cells were employed. The first type is an off-the-shelf Buchner funnel fitted with a porous glass disc (nominal pore size of 4–5 μm), and the second cell was constructed in our shop using a porous stainless steel disc (A-316L, Mott Corp.) with 0.5 μm nominal pore size.

Bubble size measurements were performed with a Coulter Multisizer instrument. Orifice tubes of 140- and 280-μm orifice diameters were used with positive polarity and a current of 1600 μA. The Coulter Multisizer stand was modified for introduction of the orifice tube directly in the flotation cell.

Figures 4a and b show two typical bubble size distributions obtained with the two flotation cells. Figure 4a, obtained with a porous glass frit at a gas flow rate of 18 mL/min, shows a gas dispersion with a mean bubble diameter of 56 μm and standard deviation of 21 μm. The finer porous steel disc, which might be expected to yield smaller bubbles, produced a gas dispersion with 77-μm mean diameter and 19-μm standard deviation at a minimum gas flow of 11 mL/min, as shown in Figure 4b. The greater hydrophobic attraction for steel than glass may have hindered detachment of smaller bubbles. The gas dispersions were characterized before each flotation run to ensure that they did not differ significantly between repeated experiments. Table 1 shows that the bubble size distributions are highly reproducible.

For a typical flotation run, an oil-in-water dispersion of twice the desired oil concentration was prepared by blending the lubricating oil with a 2% (w/v,

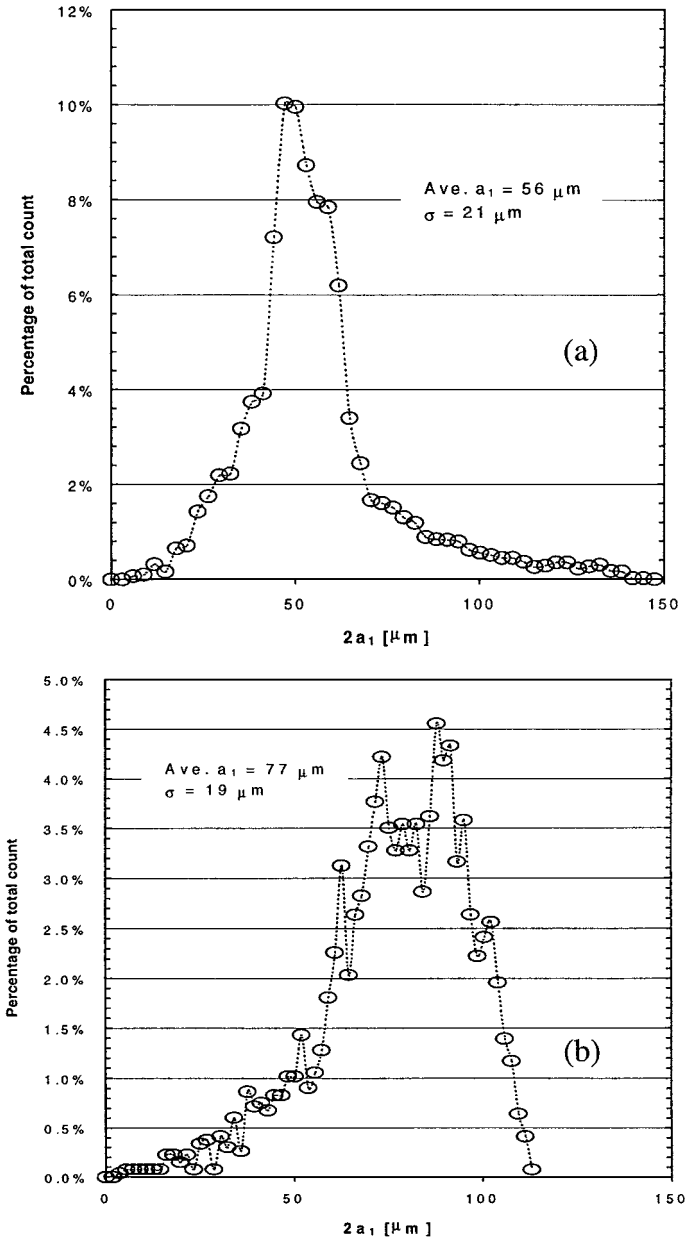

Figure 4. Typical size distributions obtained for the two different flotation cells: a) 4–5 μm porous glass disc at 18 mL/min gas flow rate; b) 0.5-μm porous stainless steel disc at 11 mL/min gas flow rate.

Marcel Dekker, Inc.
270 Madison Avenue, New York, New York 10016

Table 1. Measured Number-Averaged Bubble Diameter Plus and Minus One Standard Deviation for Separate Runs Using Glass and Steel Porous Discs

	Glass Frit at Gas Flow Rate of 18 mL/m	Steel Disc at Gas Flow Rate of 11 mL/m
Run A	56 ± 17 μm	77 ± 19 μm
Run B	56 ± 21 μm	77 ± 20 μm
Run C	N/A	76 ± 19 μm

0.35 *M*) sodium chloride (Fisher, Cat. No. S271-3) in water solution. The relatively high electrolyte concentration was used to minimize the role of bubble-droplet electrical interactions and to suppress bubble coalescence (20,21). The flotation cell was filled to half the final suspension volume with clean 2% NaCl solution, and the gas flow was started at the desired rate. After 5–10 min, when the gas flow had stabilized, isopropanol was added in the ratio 1:100 (by volume, based on the final intended volume of suspension). After manual mixing, the remaining volume was filled with the previously prepared oil-in-water dispersion, manually mixed for 10 s, and then the first measurement taken. The water temperature in all experiments was 25°C (298 K).

The suspended oil droplet count was also monitored with the Coulter Multisizer throughout each flotation run, using a 50-μm orifice tube with the same current and polarity settings as previously given. In some experiments, the rate of flotation was monitored by turbidimetry, for which a Monitek TA-1 nephelometer was employed.

For the turbidity measurements, the required sample volume of 30 mL was taken. For the droplet count measurements, suspension sample volumes of 20 mL were diluted by adding to 100 mL of clean 2% (w/v) electrolyte solution and stirring gently for 20 s. The dilution step was necessary in order to prevent inaccurate droplet counts due to coincidence-correction errors. Samples were taken at time intervals of 4 or 6 min, depending on the observed flotation rate. To minimize coalescence or creaming, the samples were analyzed immediately after being drawn and diluted.

RESULTS AND DISCUSSION

The kinetic constant for each droplet size was obtained from the slope of the natural logarithm of the drop concentration versus time. A typical plot is given in Figure 5 for four representative droplet sizes. The results show that there is good reproducibility between repeated experiments and that the kinetic constant increases with increasing drop size, as expected.

MARCEL DEKKER, INC.
270 Madison Avenue, New York, New York 10016

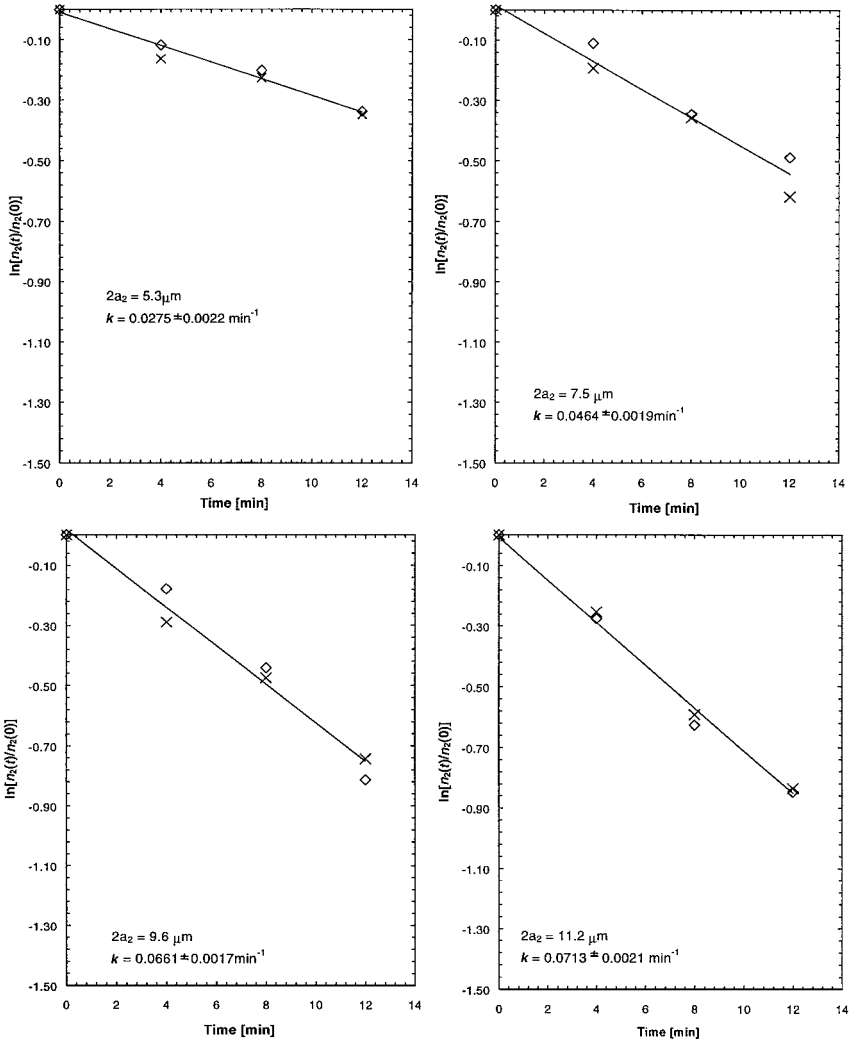

Figure 5. Natural logarithm of the droplet concentration (normalized by the initial concentration) versus time for four representative suspended droplet sizes. A gas flow rate of 18 mL/min through the glass frit was employed, resulting in a mean bubble diameter of $2a_1 = 56$ μm, and the initial oil concentration was 200 mg/L. The straight lines represent the least squares fit to the two sets of experimental data (crosses and diamonds) shown. The best-fit values and the 90% confidence intervals are shown for the kinetic constants.

MARCEL DEKKER, INC.
270 Madison Avenue, New York, New York 10016

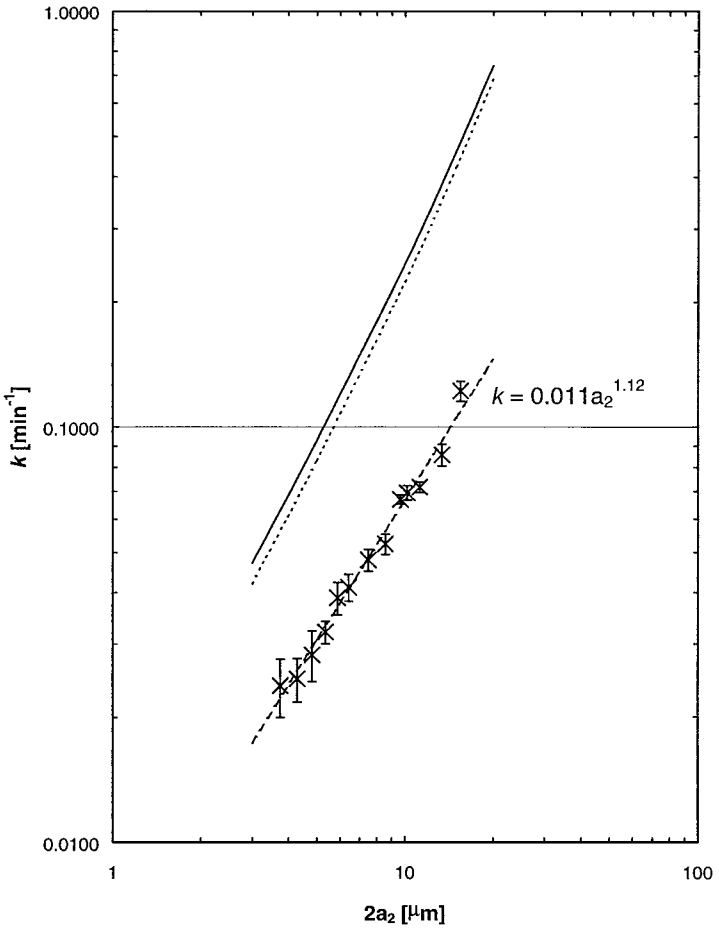

Figure 6. Comparison of measured and model-predicted kinetic constants as a function of the suspended droplet diameter for the glass frit cell, with an 18-mL/min gas flow rate and 56-μm mean bubble diameter. The solid line is the predicted kinetic constant from Equation (9), the short dashed line is the monodisperse kinetic constant from Equation (5), and the long dashed line is the least-squares linear regression of the experimental data ($\times$). Error bars represent the 90% confidence intervals on the measurements.

The measured and model-predicted kinetic constants are plotted in Figures 6 and 7 for two different bubble size distributions as a function of the suspended droplet diameter. Both theory and experiment show a strong increase in the flotation rate with increasing drop size. The smaller suspended droplets are convected more readily around the rising bubble (for these droplet dimensions, Brownian effects are

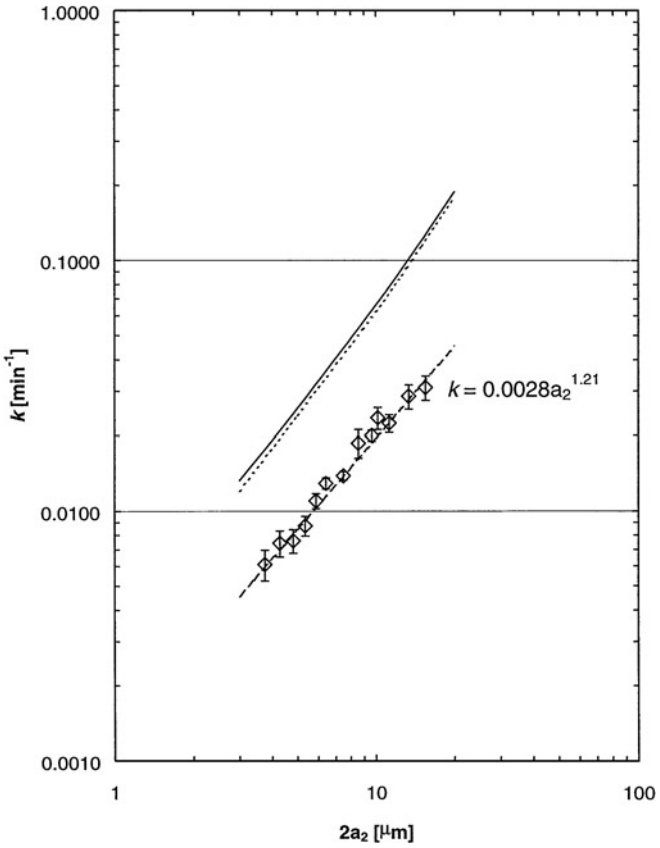

Figure 7. Comparison of measured and model-predicted kinetic constants as a function of the suspended droplet diameter for the stainless steel porous disc cell, with 11 mL/min gas flow rate and 77-μm mean bubble diameter. The solid line is the predicted kinetic constant from Equation (9), the short dashed line is the monodisperse kinetic constant from Equation (5), and the long dashed line is the least-squares linear regression of the experimental data ($\diamond$). Error bars represent the 90% confidence intervals on the measurements.

not important), thus resulting in a lower capture efficiency and lower flotation rate. However, the measured kinetic constants are approximately threefold smaller than those predicted by the theory. It may be that the surfactant led to steric hindrance to attachment when the drops and bubbles came into contact.

Comparing Figures 6 and 7 show that the larger-bubble gas dispersion results in lower rates of droplet removal. Because the larger bubbles experience higher buoyancy forces, they approach the suspended droplets at a larger velocity. This

results in a stronger convective field around the bubble, enhancing the possibility of the suspended droplets being swept past the bubble without the occurrence of a collision.

A good approximation of the predicted dependence of the flotation kinetic constant can be made by using Equation (5). As noted previously, $E_{12} \propto a_1^{-1.86} a_2^{1.21}$ and $V_{12}^o \propto a_1^2$. Then, because $n_1 = \phi/(4\pi a_1^3/3)$, where ϕ is the gas holdup, $k \propto \phi(a_1 + a_2)^2 a_1^{-2.86} a_2^{1.21}$ (or $k \propto \phi a_1^{-0.86} a_2^{1.21}$ when $a_2 \ll a_1$). The gas flow rate and holdup are related by $Q = V_1^o \phi A$, where A is the cross-sectional area of the cell and $V_1^o \approx V_{12}^o$ is the Stokes rise velocity of the bubbles. Thus, the kinetic constant is predicted to be of the form

$$k \propto Q(a_1 + a_2)^2 a_1^{-4.86} a_2^{1.21} \approx Q a_1^{-2.86} a_2^{1.21} \tag{10}$$

Thus, for a mean bubble size ratio of 56:77 and a gas flow ratio of 18:11 between the first and second sets of experimental runs, we should expect the ratio of the two kinetic constants to be 3.8, in good agreement with our measured data (compare Figs. 6 and 7).

The best linear fits to the experimental data for the two sets of experiments are also shown in Figures 6 and 7. The dependence on the suspended droplet radius follows a power relationship with exponent values of 1.1 ± 0.1 and 1.2 ± 0.1 at the 90% confidence level for the glass and metal fits, respectively. These values are in contrast to previously published results (8,9), where the observed functionality was of the form $k \propto a_2^{1.5}$. However, these previous studies were performed at rather low ionic strengths; thus, the influence of electrostatic interactions cannot be ruled out. On the other hand, our theoretical model yields the exponent 1.21 for the suspended droplet diameter, in good agreement with previous theoretical studies (1,16) and with the linear fits of the data in Figures 6 and 7.

CONCLUDING REMARKS

A quantitative comparison between the microflotation kinetic constants predicted by a trajectory analysis and those measured from batch experiments of small oil droplets in the presence of a frothing agent and salt has been performed. Over the range of drop and bubble sizes employed, the trajectory analysis with complete hydrodynamic interactions and van der Waals attractions predicts that the kinetic constant scales as $k \propto \phi a_1^{-0.86} a_2^{1.21}$ for droplets (or particles) that are much smaller than the bubbles, where ϕ is the gas holdup, a_1 is the bubble radius, and a_2 is the drop radius. Thus, smaller bubbles collect the droplets more efficiently in microflotation, and the collection efficiency increases with increasing droplet size. The experimental data support these scalings, but the measured kinetic constants are smaller than the predicted values by about a factor of three.

MARCEL DEKKER, INC.
270 Madison Avenue, New York, New York 10016

ACKNOWLEDGMENTS

This work was supported by grant CTS-9416702 from the National Science Foundation.

REFERENCES

1. Loewenberg, M.; Davis, R.H. Flotation Rates of Fine, Spherical Particles and Droplets. Chem. Eng. Sci. **1994**, *49*, 3923–3941.
2. Rubin, A.J.; Cassell, E.A.; Henderson, O.; Johnson, J.D.; Lamb, J.C. Microflotation: New Low-gas Flow Rate Foam Separation Technique for Bacteria and Algae. Biotech. Bioeng. **1966**, *8*, 135–151.
3. DeVivo, D.; Karger, B.L. Studies in the Flotation of Colloidal Particulates: Effects of Aggregation in the Flotation Process. Sep. Sci. **1970**, *5*, 145–167.
4. Rubin, A.J.; Erickson, S.F. Effect of Coagulation and Restabilization on the Microflotation of Illite. Water Res. **1971**, *5*, 437–444.
5. Cassell, E.A.; Matijevíc, E.; Mangravite, F.J.; Buzzell, T.M.; Blabac, S.B. Removal of Colloidal Pollutants by Microflotation. AIChE J. **1971**, *17*, 1486–1491.
6. Roberts, K.; Barla, P. The Influence of Lignin Sulphonate and Xylan on the Microflotation of Microcrystalline Cellulose. J. Colloid Interface Sci. **1974**, *49*, 75–81.
7. Shea, P.T.; Barnett, S.M. Flotation Separation Using Microgas Dispersions. Sep. Sci. Technol. **1979**, *14*, 757–767.
8. Reay, D.; Ratcliff, G.A. Experimental Testing of the Hydrodynamic Collision Model of Fine Particle Flotation. Can. J. Chem. Eng. **1975**, *53*, 481–486.
9. Collins, G.L.; Jameson, G.J. Double-layer Effects in the Flotation of Fine Particles. Chem. Eng. Sci. **1977**, *32*, 239–246.
10. Angelidou, C.; Keshavarz, E.; Richardson, M.J.; Jameson, G.J. The Removal of Emulsified Oil Particles from Water by Flotation. Ind. Eng. Chem. Process Des. Dev. **1977**, *16*, 436–441.
11. Reay, D.; Ratcliff, G.A. Removal of Fine Particles from Water by Dispersed Air Flotation: Effects of Bubble Size and Particle Size on Collection Efficiency. Can. J. Chem. Eng. **1973**, *51*, 178–185.
12. Rulev, N.N.; Ososkov, V.K.; Skrylev, L.D. Capture Efficiency of Small Petroleum Emulsion Droplets by Air Bubbles during Flotation. Colloid J. USSR **1977**, *39*, 522–526.
13. Okada, K.; Akagi, Y.; Yoshioka, N. Effect of Zeta Potentials of Oil Droplets and Bubbles on Flotation of Oil-in-Water Mixtures. Can. J. Chem. Eng. **1988**, *66*, 276–281.

14. Medrzycka, K.B. The Removal of Emulsified Oil Particles: Verification of the Flotation Model Based on Interception. Sep. Sci. Technol. **1993**, *28*, 1379–1394.
15. Davis, R.H. The Rate of Coagulation of a Dilute Polydisperse System of Sedimenting Spheres. J. Fluid Mech. **1984**, *145*, 179–199.
16. Ramirez, U.A.; Zinchenko, A.Z.; Loewenberg, M.; Davis, R.H. The Flotation Rates of Fine Spherical Particles under Brownian and Convective Motion. Chem. Eng. Sci. **1999**, *54*, 149–157.
17. Ramirez, J.A.; Davis, R.H. Mass Transfer to a Surfactant-Covered Bubble or Drop. AIChE J. **1999**, *45*, 1355–1358.
18. Ramirez, J.A.; Davis, R.H.; Zinchenko, A.Z. Microflotation of Fine Particles in the Presence of a Bulk-Insoluble Surfactant. Int. J. Multiphase Flow **2000**, *26*, 891–920.
19. Cassell, E.A.; Kaufman, K.M.; Matijević, E. The Effects of Bubble Size on Microflotation. Water Res. **1975**, *9*, 1017–1024.
20. Lessard, R.R.; Zieminski, S.A. Bubble Coalescence and Gas Transfer in Aqueous Electrolyte Solutions. Ind. Eng. Chem. Fund **1971**, *10*, 260–269.
21. Craig, V.S.J.; Ninham, B.W.; Pashley, R.M. The Effect of Electrolytes on Bubble Coalescence in Water. J. Phys. Chem. **1993**, *97*, 10192–10197.

Received December 30, 1999
Revised May 2000

Request Permission or Order Reprints Instantly!